Journal of Metals, Materials and Minerals, Vol.29 No.1 pp.78-85, 2019

Influences of chemical composition, microstructure and bandgap energy on photocatalytic and antimicrobial activities of ZnO and Ag-doped ZnO by solution combustion technique

Oratai JOONGPRATEEP[1,2], Kornkamon MEESOMBAD[1,*], Ratchatee TECHAPIESANCHAROENKIJ[1,2] Krissada SUWANTHANAWISES[1], Patcharaporn SIWAYAPRAHM[3], and Phonphan WATTHANARAT[3]

[1]*Department of Materials Engineering, Faculty of Engineering, Kasetsart University, Bangkok, 10900, Thailand.*
[2]*Materials Innovation Center, Faculty of Engineering, Kasetsart University, Bangkok, 10900, Thailand.*
[3]*Department of Microbiology, Faculty of Science, Kasetsart University, Bangkok, 10900, Thailand.*

***Corresponding author e-mail:** fengotj@ku.ac.th, kornkamon.mee1@ku.th

Received date:
29 September 2018
Revised date:
18 December 2018
Accepted date:
19 December 2018

Keywords:
Combustion synthesis
Nanoparticle
Ag doped ZnO
Photocatalytic activity

Abstract

Antibacterial agents, self-cleaning materials, H_2 generators and air purifiers are among common applications of photocatalysts. ZnO is a low cost material with prominent photocatalytic performance. It is generally accepted that enhancement of photocatalytic activities of powders can be achieved through doping, particle refinement, as well as tailoring of bandgap energy. It has been reported that proper doping of zinc oxide by silver lead to reduction of bandgap energy, promoting electron and hole generation, which results in enhanced photocatalytic performance. The present study aims at synthesizing ZnO and ZnO doped with 2.5, 5, and 10 mol% Ag by solution combustion technique. Influences of chemical composition, microstructure, and bandgap energy on photocatalytic activities were also examined. Compositional analysis revealed an increasing trend of Ag phase formation with greater doping content. Microstructural examination indicated that all powders contained fine particles, which agglomerated into non-uniformed clusters with average sizes ranging from 99 to 255 nm. Values of optical bandgap ranging from 3.40 to 3.22 eV were observed. The greatest and the least amount of photocatalytic degradation of methylene blue, examined at wavelength closed to 290 nm in 90 min, were found in ZnO with 2.5 mol% Ag and ZnO with 5 mol% Ag, respectively. The antibacterial activity of the powders revealed the same trend as that of the photocatalytic degradation. The antibacterial activity of the powders revealed the same trend as that of the photocatalytic degradation, with the maximum *Staphylococcus aureus* reduction of 93.88% in ZnO powder with 2.5 mol% Ag.

1. Introduction

Attributed to attractive characteristics including low toxicity, low cost and high reactivity, zinc oxide (ZnO) is exploited in numerous photocatalytic applications such as antimicrobial activity and water splitting [1,2]. To achieve extraordinary performance in the practical applications, superior photocatalytic activity is required. Mechanisms related to photocatalysis generally consisting of generation of electrons and holes. While the electrons interact with oxygen to generate superoxide radical ($\cdot O_2$), hydroxyl radicals ($\cdot OH$) are created as a result of reactions between holes and water. Both superoxide and hydroxyl radicals are active species capable of decomposing organic materials and dyes, as well as disinfecting microorganisms, hence, play an important role in performance enhancement of the photocatalysts [3].

Enhancement of electron and hole generation as well as inhibition of electron-hole recombination, therefore, are primary objectives in improvement of electrocatalytic performance of the materials. One of the limitations in zinc oxide exploitation as photocatalyst is high electron-hole recombination. It has been reported that doping zinc oxide with silver, platinum, titanium and gold inhibited electron and hole recombination [4-7].

By doping zinc oxide with silver with low doping content, oxygen vacancy defects are generated. The defects can play a role as electron traps, which prevents the recombination of electron-hole pairs.

DOI: 10.14456/jmmm.2019.12

In addition, formation of heterostructure occurs as a result of doping. The heterostructure are reported to promote electron generation and create energy barrier which prevents electron-hole recombination [8].

Numerous studies have reported photocatalytic performance of silver-doped zinc oxide. According to Abdelsamad et al. Ag-doped zinc oxide film prepared by sol-gel technique demonstrated decent performance in organic decomposition due to reduced bandgap energy and enhanced surface [9]. Nevertheless, according to Lam et al. excessive silver content could lead to diminished photocatalytic efficiency. The study indicated that high doping contents result in formation of Ag precipitates which coat the surface of particles and obstruct reaction sites [10]. The previous studies, therefore, infer that in addition to tailoring carrier generation and their recombination, control of chemical composition of the materials is required to achieve superior photocatalytic performance.

It has been widely documented that microstructural control is also a common route to accommodate photoctalysis. For photocatalytic materials in powder form, fine particles enhance reactive sites and consequently leads to improved photocatalysis and antimicrobial performance [11]. Surface enhancement and microstructural control of photocatalytic powders can be achieved via appropriate powder synthesis techniques. A number of techniques including sol gel, co-precipitation, hydrothermal, and solution combustion, exhibit the capability to produce nanoparticulate oxide powders [12-15]. In this study, solution combustion technique was employed in powder preparation process due to simplicity, rapidity, eco-friendliness, cost and energy efficiency [16].

The present study aims at synthesizing ZnO and ZnO doped with 2.5, 5, and 10 mol% Ag by solution combustion technique. Influences of chemical composition, microstructure, and bandgap energy on photocatalytic and antibacterial activities were also examined.

2. Experimental

2.1 Preparation of ZnO and Ag-doped ZnO

Zinc oxide and Ag-doped zinc oxide powders, with 2.5, 5, and 10 mol% Ag, were synthesized by solution combustion technique. While zinc nitrate hexahydrate ($Zn(NO_3)_2{\cdot}6H_2O$, Daejung®, 98%) and silver nitrate ($AgNO_3$) (GEMChem, 99.9%) were used as oxidizer, while Glycine ($C_2H_5NO_2$, Deajung) acted as combustion fuel. The oxidizer and fuels were prepared into 1.22 M aqueous solution, which was subsequently heated at 400°C to initiate combustion. The powders obtained from combustion were calcined at 450°C for 4 h.

2.2 Characterization

An x-ray diffractometer (Philips, X'Pert) was employed in phase identification, semi-quantitative analysis and determination of crystallite size of the powders. Diffraction was performed at 2 theta ranging from 20° to 80° at the scan rate and step size of $1.33°{\cdot}min^{-1}$ and 0.021 degree respectively. The content of secondary phase was calculated according to Klug's equation:

$$f_1 = \frac{(I_1^{mix}/I_1^{pure})A_2}{A_1-(I_1^{mix}/I_1^{pure})(A_1-A_2)} \quad (1)$$

where I_1^{mix} and I_1^{pure} are the phase 1 intensities in the mixture and pure material, respectively, and A_1 and A_2 are the mass absorption coefficients of primary phase and secondary phase, respectively. The average crystallite size was determined according to Scherrer's equation:

$$D_p = \frac{0.9\lambda}{\beta cos\theta} \quad (2)$$

where D_p is the mean diameter of particles (nm), λ is wavelength of the x-ray beam (0.154 nm for CuK_α radiation), β is the line broadening at half the maximum intensity (Full width at half maximum, FWHM) of the most prominent diffracted peak, and θ is the Bragg- angle.

The morphologies of the synthesized particles were examined by a scanning electron microscope (SEM) (FEI, Quanta 450). Sputtering of the powder with gold was conducted prior to the microstructural examination. The Image J Software was employed in analysis of cluster sizes.

Optical absorption spectra of the samples were measured by UV-vis spectrophotometer (Shimadzu, UV-1700 PharmaSpec) in the range 250-800 nm was employed in determination of optical bandgap of the synthesized powders. Sample preparation for the UV-vis examination was achieved by mixing the calcined powders, polyethylene glycol (PEG) (Chemipan Corporation Co., Ltd) and TritonX1000

(Applichem Panreac) together with the ratio of powder: PEG: Tritonx1000 = 1:5:0.5. The mixture was subsequently painted onto a glass substrate and heated at 400ºC for 1 h. The bandgap is determined according to the Tauc's relationship:

$$(\alpha h\nu)^2 = h\nu - E_g \quad (3)$$

where α is optical absorption coefficient, h is the Planck constant: 6.626×10^{-3} Js and ν is the wave frequency.

Photocatalytic performances of the synthesized powders were evaluated by the decomposition of methylene blue solution under UVA radiation, using QUV apparatus (Q-LAB) at the irradiance of 0.44 $W \cdot m^{-2}$ and wavelength of 340 nm. Preparation of the solution for the photocatalytic analysis was achieved by mixing 5 ppm of solution of methyl blue dye and 0.1 grams of the synthesized powders. Absorption spectra from UV-VIS spectrophotometer were obtained at the wavelength ranging from 200 to 800 nm.

Decomposition of methylene blue was conducted at 90 min using absorbance results from the UV-Vis spectrophotometer. Percent of methylene blue degradation was calculated using the following equation:

$$\% \text{ Degradation} = \left(\frac{(A_0 - A_t)}{A_0}\right) \times 100 \quad (4)$$

where A_o is the absorbance at time t = 0 min and A_t is the absorbance at t = 90 min after decomposition. The antibacterial activity against *Staphylococcus aureus* (*S. aureus*) strain ATCC6538 was determined. Single colonies were prepared by streaking bacterial strain on culture medium plate (Tryptic Soy Agar, TSA) and incubated at 37°C for 24 h. Saline suspension of single bacterial colony was prepared and adjusted to attain 0.5 McFarland turbidity standard (approximately 1.5×10^8 CFU·mL^{-1}) and then diluted the bacterial suspension to obtain 10^4 CFU·mL^{-1} for antibacterial testing. The synthesized Ag doped ZnO powders with concentration of 150 ppm were mixed with the culture medium, autoclaved at 121°C for 15 min and poured into a sterile petri plate. The 0.1 mL volume of the diluted cell suspension was spread onto the surface of a TSA medium using spread plate technique and inbubated at 37°C for 24 h. The number of bacterial colonies on the TSA plates were counted and calculated.

3. Results and discussion

3.1 Chemical composition

As shown in Figure 1, undoped powder showed single phase corresponding to hexagonal ZnO (JCPDF: 079-0207). For the powder doped with Ag, silver precipitate (JCPDS: 04-0783) was observed. Formation of the silver phase was attributed to ionic radii mismatch of the silver ion and zinc ion. In general, substitution of ion is accommodated when the ionic radii are in close proximity.

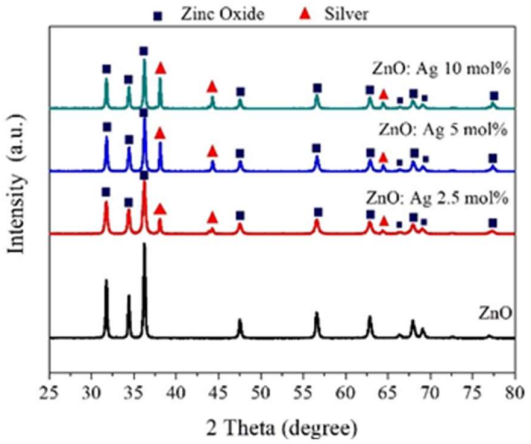

Figure 1. X-ray diffraction patterns of (a) ZnO and Ag doped ZnO powder with (b) 2.5 (c) 5 and (d) 10 mol%.

While ionic radius of the silver ion is 1.22 Å, the radius of zinc ion is 0.74 Å [17]. The large difference resulted in low solubility limit. According to Bechambi et al., Khan and Khan and Wang et al. solubility limit of silver in ZnO is 2-4 mol% [18- 20]

A semi-quantitative analysis, according to Klug's equation, was conducted. The quantity of Ag secondary phase increased with Ag doping content. The results revealed that Ag secondary phase contents in the synthesized powders of 2.3, 3.8, and 5.0 wt%, corresponding to 2.82, 4.57, and 6.25 mol %, were evident in the powders with Ag doping content of 2.5, 5, and 10 mol%, respectively.

Compositional difference generally affects catalytic performance of the materials. It has been reported that zinc oxide has relatively wide bandgap and high charge carrier recombination rate, which result in a detrimental effect in photocatalysis. Doping of zinc oxide with silver has been reported to influence photocatalytic performance. According to Georgekutty et al. silver secondary phase was

observed as a result of silver doping. At the doping content of 3 mol% Ag, methylene blue degradation increased 5 folds when compared with the undoped zinc oxide [7]. Exceedingly high Ag doping content, on the contrary, results in inferior photocatalytic performance. This is attributed to the assumption that silver phase located at the surface of zinc oxide particles functions as charge carrier recombination sites, which reduces active electrons and consequently photocatalytic efficacy [21].

In this study, silver secondary phase also formed as result of silver doping. Influence of the doping on photocatalytic performance would be discussed in the subsequent section.

3.2 Microstructure

Zinc oxide, with the hexagonal wurtzite structure, appears in various morphologies including rod-like, dumbbell, plate-like, cuboid and flower-like shape [22]. Different morphologies and sizes of the particles influence photocatalytic and antimicrobial performance of the materials. This is attributed to different surface area and reactive sites. A relationship among morphology, particle sizes and photocatalytic performance of zinc oxide doped with silver were previously reported. According to Pathak et al., flower-like structure ZnO doped with silver with an average particle size of 300 nanometers exhibited an ability to degrade 45% of organic dye in 160 min [21]. In contrast, nanofibers with the much smaller size, ranging from 14 to 19 nm, are capable of degrading more than 90% of organic dye in 70 min [23].

In this study, scanning electron micrographs revealed particles with platelet morphology, as shown in Figure 2. As silver doping content increased, particle shape was inclined to be more platelet-like. The observation was being agreed with the study conducted by Turkyilmaz et al., which reported that substitution of silver into lattice site of zinc ion accommodated coarsening along a and b axis [22].

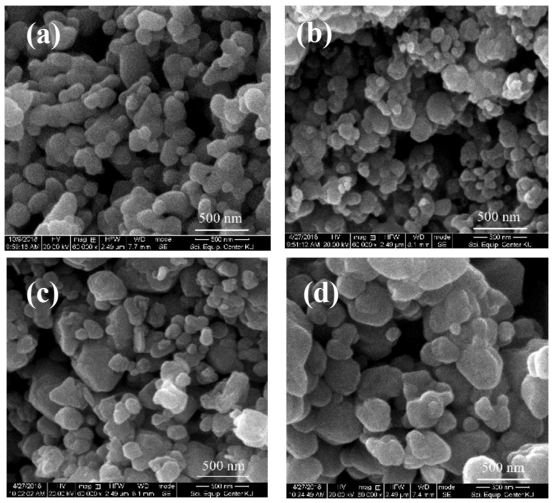

Figure 2. SEM micrographs showing particle morphology of (a) ZnO, Ag doped ZnO powder with (b) 2.5 (c) 5 and (d) 10 mol%.

Crystallite and cluster sizes were evaluated through Scherrer's equation and image analysis technique, respectively. According to Scherrer's equation, the average crystallite size was in the range between 21.7 and 81.2 nm, as shown in Table 1. The scanning electron micrographs revealed that the crystallite agglomerated into non-uniformed sized clusters with average sizes ranging from 99 to 255 nm. The finest and the coarsest crystallites and clusters were found in ZnO doped with 2.5 mol% Ag, and undoped ZnO, respectively.

Table 1. Crystallite sizes of ZnO and Ag doped ZnO powders determined from Scherrer's equation and image analysis and their average cluster sizes.

Sample	Crystallite size (nm) Scherer's equation	Crystallite size (nm) Image J	Cluster size (nm)
ZnO	81.20	97.84	255.12
ZnO:Ag 2.5	21.65	25.86	98.92
ZnO:Ag 5	28.81	38.12	115.83
ZnO:Ag 10	31.81	75.86	187.35

Refinement of crystallites in zinc oxide with low silver doping content might be attributed to the mechanism similar to Zener Pinning. Creation of defects, specifically oxygen vacancy, is commonly observed in zinc oxide doped with silver. The defects can play a role in grain boundary pinning, inhibiting grain growth [24,25]. In addition, Ag precipitates which locate along grain boundaries might also accommodate pinning effects. A similar observation has been reported by Amornpitoksuk et al. [3], which indicated that Ag doped with 1 mol% Ag, could result in particle refinement. This was attributed to inhibition of grain boundary migration caused by silver particles.

With relatively small sizes, powders obtained from this study revealed good potential to perform high photocatalytic activity. Influence of the microstructure on photocatalytic performance would be discussed in the subsequent section.

3.3 Bandgap energy

Results from bandgap energy determination revealed the values ranging from 3.22 to 3.42 eV, which is in a comparable range with several reports [26]. The results indicated that relatively low bandgap energy were observed in the zinc oxide powders with 2.5 and 5 mol% Ag

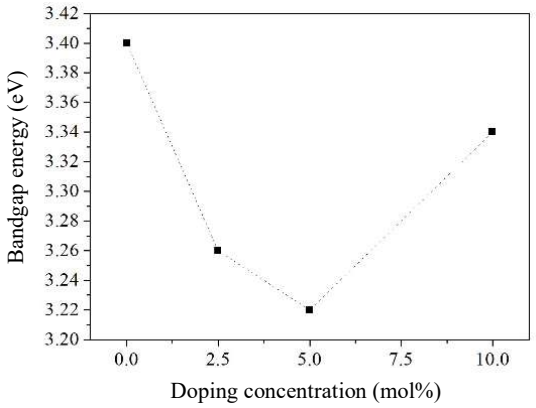

Figure 3. Bandgap energy of Ag doped ZnO powders.

Table 2. Antibacterial activity of of ZnO and Ag doped ZnO powders.

Sample	% Reduction of gram-positive *S. aureus* colonies
ZnO	85.26
ZnO:Ag 2.5 mol%	93.88
ZnO:Ag 5 mol%	78.41
ZnO:Ag 10 mol%	77.52

At the lower silver doping concentration, bandgap energy tends to decrease, shown in Figure 3. Ag doping resulted in an orbital overlap between Ag 4d and O 2p, leading to minimization of Fermi energy, as reported by Thomas et al. and Yan et al. Nevertheless, as the doping content increased, bandgap energy increased, as shown in Table 2. The observation might be explained by Moss–Burstein effect, which involves the creation of electron concentrations exceeding the conduction band edge density of states. The electrons populate within the conduction band and contributes to the shift of Fermi level to higher energy. In this case, the apparent bandgap is the combination between actual bandgap and Moss-Burstein shift [27].

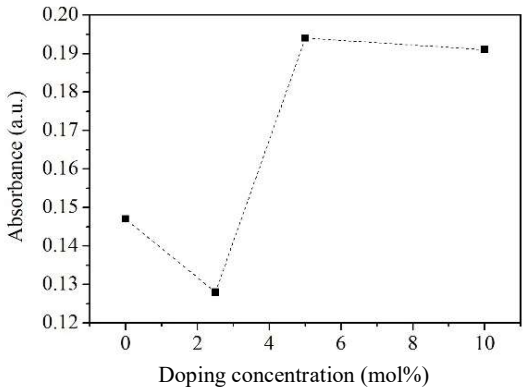

Figure 4. Absorbance vs doping concentration of Ag doped ZnO.

3.4 Photocatalytic degradation of methylene blue

Results from UV-vis spectrophotometer revealed the lowest light absorbance in the suspension containing zinc oxide with 2.5 mol% Ag. The results also indicated that the powder with 2.5 mol% Ag doped demonstrated the most prominent photocatalytic performance with 89.76% of methylene blue degradation in 90 min.

It is accepted that photocatalysis associates with microstructure and electron ic properties of the materials. Superior photocatalytic performance is generally observed in the materials with high surface area and narrow bandgap. In this study, as shown in the previous sections, the finest cluster size was found in the powder with 2.5 mol% Ag, while the relatively narrower bandgap was observed in the powder with 2.5 and 5 mol% Ag.

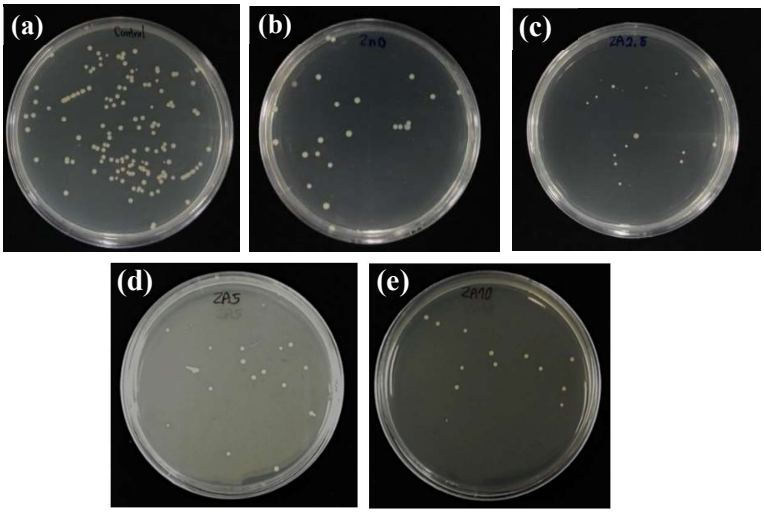

Figure 5. Antibacterial test of powders with compositions: (a) control (b) ZnO and Ag doped ZnO powder with (c) 2.5 (d) 5 and (e) 10 mol%.

Recombination rate of the electron-hole is also a factor affecting photocatalysis. At low silver doping content, oxygen vacancy can play a role as electron traps, which prevent the recombination of electron-hole pairs. However, at higher doping content, silver can function as recombination center. Georgekutty et al. has reported that silver acted as recombination center the doping concentration closed to 3 mol% [7]. High electron-hole recombination in the powders with 5 mol% Ag, thus, might be possible in this study. In addition, excessive silver content could lead to formation of Ag precipitates on surface of particles, which obstruct reaction sites. With high carrier recombination and diminished reaction sites, lower photocatalytic efficacy could be observed in the powders with 5 and 10 mol% Ag.

3.5 Antibacterial activity assay

Reduction of gram-positive *S. aureus* colonies was determined. As the synthesized powders with concentration of 150 ppm were added, the number of bacterial colonies on the plates were distinctively diminished, as shown in Figure 5. Experimental results revealed percent reduction of bacterial colonies in the range between 77.52 and 93.88%, with the highest number of colonies reduction in zinc oxide with 2.5 mol% Ag, as shown in Table 2. The antibacterial results were in agreement with the photocatalytic degradation of methylene blue; the powders with superior dye degradation tended to exhibit better antibacterial performance. Since bacterial disinfection is generally attributed to destruction of proteins at outer layers of the bacterial cell by reactive species such as $\cdot O_2^-$ and $\cdot OH$, the powders with high photocatalytic performance generally exhibit superior antibacterial activity.

3.6 A relationship among doping content, chemical composition, microstructure, bandgap energy, dye degradation, and antimicrobial activity

In general, doping contents influence chemical composition, microstructure, as well as bandgap energy of materials, which consequently affect photocatalytic performance of the materials.

In this study, zinc oxide powders with 2.5 mol% silver exhibited the best photocatalytic performance. This was attributed to proper content of secondary phase, particle sizes and bandgap energy. With 2.5 mol% Ag doping, less than 5 mol% of Ag secondary phase was formed. Presence of low quantity of secondary phase might acts as charge carrier recombination inhibitor. The 2.5 mol% Ag doped powder also exhibit particle refinement and relatively small cluster sizes, which contributed to enhanced reactive sites and consequent beneficial photocatalytic effects. In addition, relatively narrow bandgap, which was observed in the ZnO powder with 2.5 mol% Ag, could accommodate charge carrier generation and resulted in enhanced photocatalytic activities, specifically dye degradation, and antimicrobial performance.

4. Conclusions

Powders of ZnO and ZnO doped with 2.5, 5, and 10 mol% Ag were synthesized by solution combustion technique. A single phase of ZnO was observed in the undoped powder, while Ag secondary phase was present in the Ag-doped powders. The semi-quantitative analysis revealed the lowest secondary content in the ZnO doped with 2.5 mol% Ag. Agglomeration of the powders into clusters with average sizes ranging from 99 to 255 nanometers was observed. The finest clusters were found in ZnO doped with 2.5 mol% Ag. Values of optical bandgap ranged from 3.40 to 3.22 eV, with narrower bandgap observed in ZnO doped with 2.5 and 5 mol% Ag. The greatest photocatalytic degradation of methylene blue was evident in ZnO with 2.5 mol% Ag. Antimicrobial activity of the powders revealed the same trend as that of the photocatalytic degradation. Prominent photocatalytic and antimicrobial performance of the ZnO with 2.5 mol% Ag powder might be attributed to fine cluster sizes, low quantity of Ag secondary phase, and relatively narrow bandgap.

5. Acknowledgements

The authors would like to thank Kasetsart University Research and Development Institute for financial support. Equipment supports from the Department of Materials Engineering, Faculty of Engineering, Kasetsart University are also acknowledged. Valuable suggestions and fruitful discussion from Asst. Prof. Chatchawal Wongchoosuk, and Asst. Prof. Maythee Saisriyoot are gratefully acknowledged.

References

[1] H. Asadi, "Effect of calcination temperature on antimicrobial properties of ZnO/Ag nanocomposite incorporated in architectural paints," *Indian Journal of Fundamental and Applied Life Sciences,* vol. 4, pp. 315-319, 2014.

[2] J. C. Colmenares, R. Luque, J. M. Campelo, F. Colmenares, Z. Karpiński, and A. A. Romero, "Nanostructured photocatalysts and their applications in the photocatalytic transformation of lignocellulosic biomass: An Overview," *Materials*, vol. 2, pp. 2228-2258, 2009.

[3] P. Amornpitoksuk, S. Suwanboon, S. Sangkanu, A. Sukhoom, N. Muensit, and J. Baltrusaitis, "Synthesis, characterization, photocatalytic and antibacterial activities of Ag-doped ZnO powders modified with a diblock copolymer," *Powder Technology*, vol. 219, pp. 158-164, 2012.

[4] T. Welderfael, O. P. Yadav, A. M. Taddesse, and J. Kaushal, "Synthesis, characterization and photocatalytic activities of Ag-N-codoped ZnO nanoparticles for degradation of methyl red. Bull," *Chemical Society of Ethiopia*, vol. 27, pp. 221-232, 2013.

[5] S. Khosravi-Gandomani, R. Yousefi, F. Jamali-Sheini, and N. M. Huang, "Optical and electrical properties of p-type Ag-doped ZnO nanostructures," *Ceramics International,* vol. 40, no. 6, pp. 7957-7963, Jan. 2014.

[6] O. Jongprateep, P. Deedit, R. Puranasamriddhi, and K. Meesombad, "Synthesis of nanoparticulate Ti-doped ZnO by solution combustion technique," *Journal of Metals, Materials and Minerals,* vol. 28, pp. 104-108, 2018.

[7] R. Georgekutty, M. K. Seery, and S. C. Pillai, "A highly efficient Ag-ZnO photocatalyst: synthesis, properties, and mechanism," *Journal of Physical Chemistry C*, vol. 112, pp. 13563-13570, 2008.

[8] V. R. Chelli and A. K. Golder, "Ag-doping on ZnO support mediated by bio-analytes rich in ascorbic acid for photocatalytic degradation of dipyrone drug," *Chemosphere*, vol. 208, pp. 149-158, 2018.

[9] A. M. A. Abdelsamad, T. A. Gad-Allah, F. A. Mahmoud, and M. I. Badawy, "Enhanced photocatalytic degradation of textile wastewater using Ag/ZnO thin films," *Journal of Water Process Engineering,* vol. 25, pp. 88-95, 2018.

[10] S. M. Lam, J. A. Quek, and J. C. Sin, "Mechanistic investigation of visible light responsive Ag/ZnO micro/nanoflowers for enhanced photocatalytic performance and antibacterial activity," *Journal of Photochemistry and Photobiology A: Chemistry*, vol. 353, pp. 171-184, 2018.

[11] C. Karunakaran, V. Rajeswari, and P. Gomathisankar, "Combustion synthesis of ZnO and Ag-doped ZnO and their bactericidal and photocatalytic activities,"

Superlattices and Microstructures, vol. 50, pp. 234-241, 2011.

[12] S. Moradi, P. Aberoomand-Azar, S. Raeis-Farshid, S. Abedini-Khorrami, and M. H. Givianrad, "The effect of different molar ratios of ZnO on characterization and photocatalytic activity of TiO_2/ZnO nanocomposite," *Journal of Saudi Chemical Society*, vol. 20, pp. 373-378, 2016.

[13] L. Chen, B. Y. He, S. He, T. J. Wang, C. L. Su, and Y. Jin, "Fe—Ti oxide nano-adsorbent synthesized by co-precipitation for fluoride removal from drinking water and its adsorption mechanism," *Powder Technology*, vol. 227, pp. 3-8, 2011.

[14] S. J. Kwon , H. B. Im, J. E. Nam, J. K. Kang, T. S. Hwang, and K. B. Yi, "Hydrothermal synthesis of rutile–anatase TiO_2 nanobranched arrays for efficient dye-sensitized solar cells," *Applied Surface Science,* vol. 320, pp. 487-493, 2014.

[15] A. Marimuthu, and G. Madras "Photocatalytic Oxidative degradation of poly(alkyl acrylates) with nanoTiO_2," *Industrial & Engineering Chemistry Research,* vol. 47, pp. 2182-2190, 2008.

[16] O. Jongprateep, R. Puranasamriddhi, and J. Palomas, "Nanoparticulate titanium dioxide synthesized by sol–gel and solution combustion techniques," *Ceramics International,* vol. 41, pp. S169-S173, 2015.

[17] R. S. Zeferino, M. B. Flores, and U. Pal "Photoluminescence and raman scattering in Ag-doped ZnO nanoparticles," *Journal of Applied Physics,* vol.109, pp. 014308, 2011.

[18] O. Bechambi, M. Chalbi, W. Najjar, and S. Sayadi, "Photocatalytic activity of ZnO doped with Ag on the degradation of endocrine disrupting under UV irradiation and the investigation of its antibacterial activity," *Applied Surface Science*, vol. 347, pp. 414-420, 2015.

[19] G. R. Khan and R. A. Khan, "Ergonomic synthesis suitable for industrial production of silver-festooned zinc oxide nanorods," *International Journal of Nanoscience,* vol. 14, pp. 1550018, 2015.

[20] L. Wang, Q. Hu, Z. Li, J. Guo, and Y. Li, "Microwave-assisted synthesis and photocatalytic performance of Ag-doped hierarchical ZnO architectures," *Materials Letters,* vol. 79, pp. 277-280, 2012.

[21] T. K. Pathak, R. E. Kroon, and H. C. Swart, "Photocatalytic and biological applications of Ag and Au doped ZnO nanomaterial synthesized by combustion," *Vacuum*, vol. 157, pp. 508-513, 2018.

[22] S. S. Turkyilmaz, N. Guy, and M. Ozacar, "Photocatalytic efficiencies of Ni, Mn, Fe and Ag doped ZnO nanostructures synthesized by hydrothermal method: The synergistic/antagonistic effect between ZnO and metals," *Journal of Photochemistry and Photobiology A: Chemistry,* vol. 341, pp. 39-50, 2017.

[23] D. Lin, H. Wu, R. Zhang, and W. Pan, "Enhanced photocatalysis of electrospun Ag−ZnO heterostructured nanofibers," *Chemistry of Materials*, vol. 21, pp. 3479-3483, 2009.

[24] K. Ravichandran, P. Sathish, S. Snega, K. Karthika, P. V. Rajkumar, K. Subha, and B. Sakthivel, "Improving the antibacterial efficiency of ZnO nanopowders through simultaneous anionic (F) and cationic (Ag) doping," *Powder Technology*, vol. 274, pp. 250-257, 2015.

[25] K. Ravichandran, R. Rathi, M. Baneto, K. Karthika, P. V. Rajkumar, B. Sakthive, and K. Damodaran, "Effect of Fe+F doping on the antibacterial activity of ZnO powder," *Ceramics International,* vol. 41, pp. 3390-3395, 2015.

[26] Y. Jin, Q. Cui, K. Wang, J. Hao, Q. Wang, and J. Zhang, "Investigation of photoluminescence in undoped and Ag-doped ZnO flowerlike nanocrystals," *Journal of Applied Physics*, vol. 109, pp. 053521, 2011.

[27] A. Singh, D. Mohan, S. Ahlawat, and R. Richa, "Performances of spin coated silver doped ZnO photoanode based dye sensitized solar cell," *Processing and Application of Ceramics,* vol. 11, pp. 213-219, 2017.